Numerical modelling of downstream migrating antidunes

Prof. Nils Reidar B. Olsen

Department of Hydraulic and Environmental Engineering, NTNU, The Norwegian University of Science and Technology, Norway

ABSTRACT

A numerical model is presented that compute the geometrical dimensions and movement of downstream migrating antidunes. The model solves the Navier-Stokes equations together with the k-epsilon turbulence model to find the water flow field over the bedforms. A two-dimensional width-averaged grid is used. The bed elevation changes are computed by solving the convection-diffusion equation for suspended sediments and bed load, together with the Engelund-Hansen sediment transport formula. The free surface is computed with an algorithm based on water continuity in the surface cells. Non-orthogonal adaptive grids were used, moving vertically with the computed location of the bed and the free water surface. The numerical model was tested on data from a physical model study where regular downstream migrating antidunes had been observed. The numerical model started out with a flat bed and the trains of antidunes formed over time. Many of the physical processes observed in earlier studies were replicated by the numerical model. Four dune parameters were computed in the current tests: The antidune wavelength, height and celerity, together with the average water depth. The antidune

This article has been accepted for publication and undergone full peer review but has not been through the copyediting, typesetting, pagination and proofreading process which may lead to differences between this version and the Version of Record. Please cite this article as doi: 10.1002/esp.4193

wavelengths were best predicted with an accuracy of 3-8 % compared with the measurements. The antidune heights were computed with a deviation of 11-25 % compared with an empirical formula. The water depths over the antidunes were predicted with an accuracy of 3-9 % related to the measured values. The average antidune celerity was the parameter with largest deviation: For the coarsest grid it was overpredicted with 37 %.

KEY WORDS

Numerical modelling, antidunes, sediment transport, Navier-Stokes equations, adaptive grid.

INTRODUCTION

Alluvial water channels often contain some sort of bedform, for example a dune. Considerable research has been made on dunes, regarding their three-dimensional nature (Walker and Shugar, 2014), affect on energy losses in the channel (Warmink et al., 2014) as well as the sediment transport capacity (Naqshband et al., 2016). Dunes in water channels mostly occur where the Froude number is well below unity. The water level over a dune crest is then usually slightly lower than over the trough. This is due to the higher velocity over the crest, where energy is transferred from pressure/water elevation to velocity. Erosion will take place at the upstream side of the dunes, and the sediments will deposit downstream. The dunes will therefore move downstream.

Antidunes are bedforms that occur in alluvial channels with considerable sediment transport and Froude numbers near 1. Gilbert (1914) described antidunes as “sinusoidal-shaped bed features” that move in the opposite direction of the water flow, thereby giving the bedform its name. The sediment may be eroded on the downstream side of an antidune, and deposited at the upstream side of the following antidune. Thereby, the antidune would move upstream. Kennedy (1963) observed that bed forms occurring where the Froude number is close to unity also can move downstream. He therefore redefined antidunes to be characterized from the water surface profile instead of the direction of movement: “The antidunes occur when the surface gravity waves are in phase with the bedforms”. The water surface over an antidune will follow the same shape as the bed, with the lowest values over the trough and highest waterlevels over the crest. The definition by Kennedy (1963) has later been used by other researchers (Núñez-González and Martín-Vide, J. P., 2010) and it is also adopted in the current study.

A number of scientific studies have been carried out on the topic of antidunes in rivers and channels (Kennedy, 1963; Karim, 1999; Recking et al., 2009). Geologists and sedimentologists investigate antidunes as a part of step-pool sequences (Curran, 2007) or to infer lamination of sedimentary structures (Alexander et al., 2001; Yokokawa et al., 2010). Hydraulic engineers encounter antidunes when flushing sediments from water reservoirs (Haun and Olsen, 2012) or during morphological changes in the reservoir bathymetry after a dam decommissioning (Bromley, 2007). Fig. 1 shows antidunes during flushing of the Bodendorf reservoir in Austria. The antidunes will affect the energy loss of the water flow and the sediment transport capacity. Abad et al. (2014) found that ordinary dunes could completely disrupt the secondary currents in a meandering channel. It is therefore possible that

also antidunes could affect the secondary currents in channel bends during reservoir flushing. The antidunes will thereby play a role in how much sediments can be flushed from a reservoir and the bed geometry of the reservoir after the flushing. This is one of the main motivations for the current study.

A numerical model for prediction of antidune formation should in theory be most accurate if it is based on solving the Navier-Stokes equations, since these equations describe the water flow movement. Several earlier studies have been carried out where the water flow and bed level changes were computed in a river/reservoir by solving the 3D Navier-Stokes equations together with a sediment transport formula. For example, Fischer-Antze et al. (2008) computed bed level changes in the Danube river during a large flood. The main erosion and deposition pattern were reproduced. The grid was, however, too coarse to resolve individual bed forms. The dunes were modelled as a roughness for each bed cell in the grid, which is the most common approach for morphological computations over a large scale. The movement of ordinary dunes in sub-critical flow have been computed earlier using a fine grid replicating both laboratory cases (Tjerry and Fredsøe, 2005; Giri and Shimizu, 2006; Nabi et al., 2013; Lopes et al., 2013; Dore et al., 2016; Mewis, 2016) and dunes in a natural river (Ruether et al., 2008). The main problem modelling antidunes is the steep slopes of the water surface and the non-hydrostatic pressure distribution. Most general-purpose CFD models compute the free surface with a Volume of Fluid (VOF) method and a fixed grid. This requires two fluid phases: air and water. The sediments can be modelled as a third phase, but a three-phase solution of the Navier-Stokes equations is not straightforward. Many numerical models for river flow use the Shallow water equations and a hydrostatic pressure assumption. The water pressure over an antidune is highly non-hydrostatic, and it is therefore required that

the momentum equation in the vertical direction is solved. This was done in the present study, with only one phase (water and suspended sediments). A new algorithm to compute the movement of the free surface (Olsen, 2015) was used instead of the VOF method.

Olsen (2016) investigated if it was feasible to use this approach in modelling the formation of the antidunes. In the current, a longer computational domain, finer grids and longer simulation times has been used to obtain more detailed information about the antidune formation. Also, a grid sensitivity test has been carried out. A newly developed dune tracking algorithm was applied, allowing the computation of important antidune characteristics as wavelength, amplitude and water depth. The migration speed of the antidune was also determined. These parameters were compared with results from the physical model study.

One of the long-term goals of the current project is to be able to model the effect of the antidunes on secondary currents in rivers. Three-dimensional effects in formation of ordinary dunes in water channels have earlier been studied by Yokokawa et al. (2010). In the current study, only a 2D width-averaged model was used in order to reduce the computational requirements. Thereby, numerical modelling of 3D effects in antidunes is a topic left for further studies at a later stage.

LABORATORY DATA OF ANTIDUNES

Many physical model studies have been carried out on antidune formation (Cartigny et al., 2014; Curran, 2007; Alexander et al., 2001; Yokokawa et al., 2010). The current study used data from the PhD study of John F. Kennedy. Kennedy (1960) carried out 43 laboratory runs where antidunes where formed. The runs had different

sediment sizes, bed slopes, water depths and water velocities. Two different flumes were also used, where one was longer and wider than the other. Only one of these runs was selected to be simulated by the numerical model, due to the long computational time. With the finest grid, the wall time of the computing cluster was four weeks. The experiment number 5-1 (Kennedy, 1960) was chosen. A 12 meter long and 25 cm wide recirculation flume was used, where the sediments had 0.549 mm average grain size. The Froude number was 0.77, the water depth 0.105 m and the water velocity was 0.78 m/s. Well defined antidunes formed, with an average celerity of 5 mm/s (1 ft/min) and an average wavelength of 0.38 meters. The wave length of the antidunes were determining in the laboratory by measuring the streamwise distance of an integral number of waves. The most upstream 3 meters were not included in the procedure, as entrance effects were observed. A recirculating sediment feed was used in the flume, and this was also included in the numerical model. The antidunes for case 5-1 were two-dimensional, which was important when selecting this case because the numerical model was also two-dimensional. Three-dimensional effects, so called “rooster tails”, with high-amplitude waves in the middle of the channel were observed for many of the other experimental runs of Kennedy (1960). Modelling these phenomena would require a three-dimensional grid, taking considerably more computational time than what was used in the current study.

A question is how antidunes can form in an initially straight channel with a flat bed. Kennedy (1960) tried to make the upstream flow conditions in the flume as uniform as possible. This included several metal grids placed in the upstream cross-sections. The grids made the velocity profile more uniform, but they also increased the turbulence. This caused a scour hole to form downstream of the grids. To reduce the

scour hole magnitude, a tapered sill was placed on the bed in the upstream region. This reduced the scour hole magnitude. However, Kennedy (1960) stated that the formation of the antidunes was caused by the upstream perturbation of the inlet region. "If the flow was given no disturbance at the flume entrance, the bed and water surface were flat everywhere".

For the currently studied run, 5-1, Kennedy (1960) observed that the initiation of the antidunes started with ordinary small dunes on the bed. When the dunes grew larger they caused disturbances on the surface which formed surface waves. These waves then again acted on the dunes causing them to become larger. This resulted in the formation of the classical antidunes, which Kennedy (1960) described as "rounded and sinuous" in shape. The current case has a Froude number of 0.77, which is low compared with the critical flow situation. The antidune growth mechanism starting with bed dunes was observed at relatively low Froude numbers. Kennedy (1960) also carried out experiments with higher Froude numbers, and then the initial oscillations started at the water surface instead of at the bed.

NUMERICAL MODEL

The numerical model was based on a finite volume method computing the water velocities, U_i, in the *i* direction by solving the Navier-Stokes equations:

$$\frac{\partial U_i}{\partial t} + U_j \frac{\partial U_i}{\partial x_j} = \frac{1}{\rho} \frac{\partial}{\partial x_j} (-P\delta_{ij} - \rho \overline{u_i u_j}) - \mathrm{g} \qquad j=1,2 \qquad (1)$$

P is the pressure, *x* is a space direction, *t* is the time, δ_{ij} is the Kronecker delta and *g* is the acceleration of gravity. The Reynolds stress, $-\rho \overline{u_i u_j}$ was computed by the *k*-

epsilon turbulence model (Launder an Spalding, 1974). This model had previously been applied to compute the flow field over a dune (Stoesser et al., 2006) where good agreement had been found with experimental data for the velocity field. The pressure was computed using the SIMPLE algorithm (Patankar, 1980), which computes a pressure-correction from the water continuity defect in a cell. The convective term, which is the second term on the left side of Eq. 1, was discretized using a first-order upwind scheme.

Zero gradient boundary conditions were used for the channel sides, the water surface and the outflow section in the solution of the Navier-Stokes equations. Wall laws for rough boundaries (Schlichting, 1979) were used for resolving the gradients towards the bed:

$$\frac{U}{u_*} = \frac{1}{\kappa}\left(\frac{30\Delta}{k_s}\right) \qquad (2)$$

The distance from the bed to the center of the bed cell is denoted Δ. The empirical parameter κ is given as 0.4 and k_s is the roughness in meters. The roughness was computed by the formula of van Rijn (1982). The shear velocity, u_*, is defined as the square root of the bed shear stress divided with the water density. The equation gives the bed shear stress once the roughness and the velocity is computed. The bed shear stress is used as a sink term in the Navier-Stokes equations, reducing the velocity at the bed.

The sediment transport was computed by solving the transient convection-diffusion equation for the sediment concentration, *c*:

$$\frac{\partial c}{\partial t} + U_j \frac{\partial c}{\partial x_j} + w\frac{\partial c}{\partial z} = \frac{\partial}{\partial x_j}\left(\Gamma_T \frac{\partial c}{\partial x_j}\right) \quad (3)$$

The fall velocity of the sediment particles is denoted w. The turbulent diffusion coefficient, Γ_T, was set equal to the eddy-viscosity from the k-epsilon turbulence model. The velocity in Eq. 3 was taken from the solution of the Navier-Stokes equations. The equation assumes that the water and the sediments move as one phase, but that the sediment particle velocities have a constant deviation in the vertical direction compared with the water velocity. This assumption is called a drift-flux model and is taken care of with the third term on the left side of Eq. 3.

The Engelund-Hansen (1967) formula was used as a boundary condition at the bed, giving the sediment discharge, q_s, as:

$$q_s = 0.05\rho_s U^2 \sqrt{\frac{d_{50}}{g\left(\frac{\rho_s}{\rho_w} - 1\right)}} \left[\frac{\tau}{g(\rho_s - \rho_w)d_{50}}\right]^{3/2} \quad (4)$$

The particle diameter is denoted d_{50}, ρ_s is the sediment density (2650 kg/m^3), ρ_w is the density of water and τ is the bed shear stress.

The time-dependent morphological changes were done by solving the Navier-Stokes equations and computing the water flow and sediment transport for each time step. The bed changes were computed from the sediment transport results. The vertical bed changes in the centre of each bed cell were calculated from the Exner equation. This is a continuity equation where the difference between sediment inflow and

outflow in one cell is multiplied with the time step and the result is divided by the area of the cell seen from above. The resulting average bed movement in each cell was transferred to the corners of the cell, where the vertical levels of the bed were defined (Olsen, 2003).

The location of the free water surface was computed from the CGA (Continuity, Gravity Adaptive grid) method described and tested by Olsen (2015). The method uses the water continuity defect in the cells closes to the water surface to move the surface up or down a distance Δz. The pressure at the water surface is assumed to be zero, so the pressure in the cell closest to the surface is interpolated from the cell below. Not using the SIMPLE method in the cell closest to the surface gives a water continuity flux defect, ΔQ, in these cells. The water surface elevation is then updated with an increment Δz according to the following formula:

$$\Delta z = \Delta Q \Delta t / A \quad (5)$$

A is the area of the cell in projected in the horizontal plane and Δt is the time step. The formula was applied to all surface cells and thereby gave the vertical movement of the free surface. More details and test results for this numerical algorithm are given by Olsen (2015).

After each time step, the changes in the bed and water levels were transferred to the grid, which was moved and stretched or shrunk in the vertical direction. Then the velocity and sediment transport in the new time step was computed. A 2D width-averaged grid was used, which was structured and non-orthogonal. A co-located variable arrangement was used, meaning all the variables were computed in the center of the cells. The computer program could operate with a varying number of

cells in the vertical direction, but the use of a constant number avoided the use of triangular cells in the grid. Thereby, better numerical stability was observed.

The water flow module of the numerical model had been tested previously against velocity measurements for a number of cases, for example flow in a laboratory channel (Wilson et al., 2003) and over a sand dune (Stoesser et al., 2006). The free surface algorithm had also been tested earlier against laboratory experiments of a 3D weir (Olsen, 2015) and on a sand slide experiment (Olsen, 2013b). The sediment transport module had been tested against measured concentrations in the field (Haun et al., 2013), and bed elevation changes in a physical model (Olsen and Kjellesvig, 1998) and in the field (Zinke et al., 2011). The movement of ordinary dunes in sub-critical flow had also been modelled earlier and tested against field data form a branch of the delta at Lake Øyern in Norway (Ruether et al., 2008). The dune movement was then measured with a side-scan sonar. The computed and measured dune movements compared well.

A bedform tracking function was also implemented in the numerical model. At given time intervals, a specified section of the grid was analyzed and the highest and lowest points on the bed were found. The average elevation difference between the points was computed as the bedform heights. The locations of the highest points (x-value) were also saved. The average distance between the points was defined as the bedform length. Next time the tracking function was called, the new locations of the points were compared with the previous values. The average distance travelled by the bedform peaks divided by the time interval was defined as the antidune celerity. The bedform tracking function also computed the average water depth and

antidune lengths. Time series of these parameters were compared with the measured values.

The computations were then carried out on the Vilje cluster at NTNU in Trondheim, Norway. This is an SGI Altix ICE X computer with 2.6 GHz Intel Xeon E5-2670 processors. The computer program was parallelized with OpenMP. The longest run with the finest grid used a wall time of four weeks on one 16 core node of the cluster. Then the evolution and movement of the antidunes over a time period of 1000 seconds were computed.

RESULTS

The numerical model was given the geometry, water discharge and sediment data from the selected test case (Kennedy, 1960). A time step of 0.0002 seconds was used and the number of grid cells in the longitudinal direction was 2400. The number of cells in the vertical direction was 38 and 50 for two different runs. Since a 2D simulation was done, only one cell in the lateral direction was used. The grid cells had a length of 5 mm, and an average height of 2-3 mm. This meant that each antidune would be resolved with approximately 75 cells in the longitudinal direction. Fig. 2 shows a section of the grid.

Both dunes and antidunes can be seen as a type of instabilities of the channel bed. Lopez et al. (2013) specified a full sized dune at the initial bed with a sine function, and investigated how the dune moved over time. Dore et al. (2016) used small variations in the initial bed elevations at the order of the sediment size, d_{50}. The instability starts with low values and increases over time. A similar instability increase is seen in the formation of a meandering channel from an initially straight planform.

Olsen (2003) computed the meandering channel from an upstream instability while Ruether and Olsen (2007) were able to obtain meandering pattern without any perturbations in the boundary conditions. A question is therefore also how antidunes start to form. Is an upstream perturbation needed?

In the numerical model, special care had to be taken at the inlet and outlet boundary. The exact details of the inlet geometry of the flume were not given by Kennedy (1960), making it impossible to replicate the experiment exactly in the numerical model. Instead, another boundary condition was used. The vertical inlet was modelled with a horizontal inflow, but the momentum of the inflowing water was set to zero. Also a non-erodible bed was specified for the first 30 cm of the flume. This produced a small scour hole right downstream of the non-erodible section. The pertubation was similar to observations from the physical model, where a scour formed downstream of the metal grid. The initial perturbation at the inlet caused the formation of the antidunes to start from the upstream end. The perturbation is seen in Fig. 3, after 1 second. Fig. 3 shows that the perturbation progresses downstream while growing in size, in the images taken from 3-7 seconds. This bed form is essentially a small dune, as the water surface profile is relatively flat. The scour downstream of the non-erodible section increased over time, causing a deposition right downstream. A small standing surface wave formed just upstream of his deposition, as can be seen in Fig. 3. This is the start of an antidune. The perturbation of the bed and the in-phase surface wave increased in magnitude over time. The process is similar to what was observed in the laboratory model (Kennedy, 1960).

Fig. 4 shows computed longitudinal profiles of the whole length of the flume at longer time steps. The figures are distorted, as the vertical scale is multiplied with a factor 5.

The figure shows how the antidunes started from the upstream boundary and moved downstream while they increased in size. After 10 seconds, the antidunes only occur at the upstream boundary. After 100 seconds the bed perturbations covered the whole flume, but they had not yet reached their maximum size. The water surface was also not in phase with the bed. This occurred after 200 seconds. After 300 seconds, the antidunes had reached their maximum size. They continued to progress downstream. Both Fig. 4 and the observations in the laboratory experiments showed that the antidune heights and lengths varied over time.

The classical dune profile for subcritical flow will have a recirculation zone on the lee side. This is not always seen for all dunes in laboratory experiments, as it depends on the height and length of the dune. The numerical model only showed recirculation zones behind the largest antidunes. This is shown in Fig. 5, where vectors are given. The velocity pattern in the recirculation zone is similar to earlier more detailed computations of flow over regular dunes (Stoesser et al., 2006). Smaller antidunes without any downstream recirculation zone still had lower velocities at the lee side close to the bed.

Fig. 6 shows detailed velocity, pressure and concentration profiles over antidunes. The maximum velocity is located at the lowest point of the water surface, corresponding well with energy considerations and the Bernoulli equation. The potential energy from the water over the crest is transferred to velocity energy in the trough. The lowest water velocity is at the bed in the trough, where the recirculation zone may form.

Isolines of pressure are also given in Fig. 6. They are not horizontal, and they do not follow the bed or water surface. It is interesting to see that the vertical pressure

gradient is higher in the antidune troughs than at the crest. This non-hydrostatic pressure distribution makes it necessary to also solve the Navier-Stokes equations in the vertical direction to be able to compute a correct velocity field. The non-hydrostatic pressure is in correspondence with theoretical considerations by Núñez-González and Martin-Vide (2011).

Fig. 6 also shows that the sediments move mostly along the bed. The greyshading of the figure have been scaled so that the effect of the recirculaton zone downstream of the antidune crest is seen. The vertical sediment concentration gradient close to the bed is smaller in the recirculation zone than at the antidune crest, due to the upward movement of the water in the vertical direction.

Fig. 7 and 8 show time series from the results of the bedform tracking algorithm for the two vertical grids. Values for the antidune height, water depth, antidune length and celerity are produced every 4th second. The time-averaged computed and measured values are given in Table 1, where the averaging is done over the last 700 of the 1000 computed seconds. The computed antidune lengths are computed to be 35 and 37 cm for the two grids. This compares well with the observed value of 38 cm. The maximum deviation between the computed value and the measured is 8 %. Fig. 7 and 8 show that there are some fluctuations of the computed values over time. It is also interesting to see how the lengths of the antidunes develop over time. The initial antidune length is small and grows over time. This is seen both in the time series of Fig. 7 and 8, and in the longitudinal profiles of Fig. 3 and 4. The growth of the antidunes over time was also observed in the laboratory studies.

The computed water depth averaged over the last 700 seconds was 10.8 cm and 9.8 cm for the two grids. The observed average water depth was 10.5 cm. This is a

deviation of 3-11 %. The initial water depth was set equal to the measured water depth for both cases. Figs. 7 and 8 show that the average water depths first decrease at the start each computation. The specified grain roughness is not large enough to cause a friction loss that can keep the water level as high as what was given initially. However, after the antidunes have developed, the energy losses over the bed forms make the water level rise to higher values. The values then correspond better with observations from the physical model. The energy losses occur due to the contraction/expansion of the water depths over the antidunes, including recirculation zones.

The antidune celerity is given in Fig. 7 and 8 for the two grids. The celerity is highest right after the antidunes are formed, and then it is reduced. The values are fluctuating over time, and the average values do not exactly correspond to the measured celerities. The measured averaged value was 0.5 cm/s, while the computed value was 0.78 and 0.48 cm/s, averaged over the last 700 seconds of the run. However, Fig. 7 and 8 show that the computed celerity fluctuates considerably. A question is also how accurate the antidune celerity was measured. Kennedy (1960) stated that it was "around 1 foot/minute", which means it might have been slightly smaller or larger.

The computed antidune heights are also given in Fig. 7 and 8. Unfortunately, Kennedy (1960) did not measure the antidune height in his experiments. The value can, however, be estimated by empirical formulas for bedform dimensions. Most formulas are developed for ordinary dunes, but Karim (1999) also made an equation for the antidune height, h:

$$\frac{h}{d} = \left(\frac{\left[S - 0.0168 \left(\frac{d_{50}}{d} \right)^{0.33} Fr^2 \right] \left[\frac{L}{d} \right]^{1.2}}{0.085 Fr^2} \right)^{0.73} \quad (6)$$

L is the antidune length, *d* is the water depth, *S* is the slope and *Fr* is the Froude number. The average sediment diameter is denoted d_{50}. The equation gives an antidune height of 2.7 cm. This is very close to the computed values of 2.1 cm and 3.0 cm. Note that the grid with the finest resolution in the vertical direction gives the best results for this parameter.

DISCUSSION

An important parameter in all CFD computations is the grid and its size. The current study used around 75 cells in the longitudinal direction for each dune wavelength. According to Dore et al. (2016), this should be a sufficient resolution, as they found that 35 grid cells were needed to resolve one wavelength. However, Dore et al. (2016) used a third-order discretization scheme (Zijlema, 1996). The current study used a first-order upwind scheme, which induced more false diffusion than a high-order scheme. Therefore more cells were required to achieve the same accuracy. An attempt to use a second-order upwind scheme in the current study failed as too much instabilities of a regular dune pattern formed. Therefore, the first-order scheme had to be used. The grid used in the current study was non-orthogonal and adaptive so that the gridlines mostly followed the directions of the velocity vectors. This reduced the false diffusion.

Earlier studies have also been made on computing the flow field over fixed dunes. An example is Stoesser et al. (2006), who tested several turbulence models and compared velocity profiles with experiments. This study used 416 cells in the horizontal direction for each wavelength. They also used 170-192 cells in the vertical direction, which is much more than the 50 cells used in the current study.

In the current study, the effect of the grid resolution was investigated by using two grids with different vertical resolution were used: 38 and 50 cells. The results were not identical, but similar. The antidune length, the water depth and the antidune celerity was best predicted with the finest grid. The antidune length was slightly better predicted with the coarse grid. However, the results from both grids were fairly similar to the observed value. Although the antidune length was well predicted with both grids, the antidune height was much better computed with more cells in the vertical direction. The deviation between computed antidune height and the empirical formula was reduced from 25 % to 11 %, indicating that the vertical grid resolution is important for the computation of this parameter.

The effect of the grid resolution in the vertical direction can also be seen when comparing Fig. 7 and 8. The difference in time-averaged values for antidune height, water depth, antidune length and celerity corresponds well with the values given in Table 2. The antidune celerity has a much larger variation over time for the coarser grid (Fig. 7) than for the finer grid (Fig. 8). This indicates that the antidune movement was more unstable in the coarse grid than the finer grid. The more stable values in the finer grid gave a lower celerity, which corresponds better with the observed value.

The grid refinement test for the current case gave reasonable results, as most of the parameters improved with a finer grid. Olsen (2016) also computed another antidune case with a higher Froude number and coarser sediments, where experiments had been carried out by Núñez-González (2012). Then only 20 cells were used in the vertical direction, much less than the 38 - 50 cells were used in the current study. Although the dune length was well predicted with this coarse grid, the dune height was considerably underpredicted. Grid sensitivity tests for the Núñez-González case with increased number of cells in the vertical direction this did not produce improved results. A possible reason for this could be instabilities, as the Froude number of the Núñez-González case was higher (Fr=0.97) than the current case (Fr=0.77). Another possible reason is that the Núñez-González case had three times larger sediment particles than the 5-1 case, meaning the roughness height was 1 cm. Since the water depth was around 10 cm for both cases, the cell size was 5 mm with 20 cells over the depth. The roughness was therefore considerably higher than the bed cell, and would protrude into multiple cells above the bed cell. The effect of the bed roughness in the current model only affected the bed cell. A solution to this problem is to develop boundary conditions for situations where the roughness is much larger than the bed cells. This is a topic for further studies.

An important parameter for transient CFD computations is the time step. In the current study, this parameter was determined by trial and error. The value of 0.0002 seconds gave stable results with a smooth water surface. Increasing the time step to 0.0004 seconds gave oscillations at the water surface. This is seen in Fig. 9.

In the current case, the antidunes have moved downstream. Upstream moving antidunes are more difficult to model numerically, as they are much more unstable.

They may also break, which is a rapid unsteady process with air entrainment and a very complex water surface. This is a more complex problem then the downstream migrating antidunes studied in the current study, and therefore also a topic for future research.

CONCLUSIONS

A CFD model solving the Navier-Stokes equations together with a convection-diffusion equation for sediment transport has been able to compute the formation of downstream migrating antidunes. A free surface algorithm based on the water continuity was successfully able to model the antidune water wave. The drift-flux sediment model with a movable bed also predicted the downstream movement of the antidunes.

The numerical model predicted the formation process of the antidunes starting from a flat bed with an upstream disturbance. This corresponds with observations from the flume experiment by Kennedy (1960). The initial bed perturbations formed in the numerical model were small and grew in size both in the vertical and longitudinal direction. This was also observed in the physical model studies.

The profiles of the computed pressure over the dunes are strongly non-hydrostatic, corresponding with theoretical considerations by Núñez-González and Martin-Vide (2011). Also, recirculation zones behind the larger antidunes were computed by the numerical model. This shows that the numerical model is able to replicate many of the physical processes in the formation of the antidunes.

One of the purposes of the current study was to see how well the numerical model was able to predict characteristic antidune parameters: water depth, antidune height,

antidune length and antidune celerity. All parameters were computed within a deviation of 11 % for the finest grid. The antidune lengths were computed with an accuracy of 3-9 % compared with the physical experiments. The antidune heights were computed with an accuracy of 11-25 % compared with an empirical formula. The water depth computed by the numerical model results from a determination of the skin friction of the sediment particles on the bed in combination with bulk energy losses over the dunes. The water depth was computed with an accuracy of 3-9 % compared with the physical model results. The dune celerity was computed with an accuracy of 4-37 %, compared with the experiments. However, this parameter also has large variations over time and space, and may not have been very accurately estimated in the laboratory experiments.

ACKNOWLEDGEMENTS

I want to thank Dr. Francisco Núñez-González for interesting discussions about antidunes and for information about his laboratory experiments. This research was supported in part with computational resources at NTNU provided by NOTUR, http://www.notur.no. I want to thank Vegard Eide at the High Performance Computing Centre at NTNU for help in allowing the computations to exceed the maximum wall time limit of the cluster.

REFERENCE LIST

Abad, J. D., Frias, C. E., Buscaglia, G. C., Garcia, M. H. 2014. Modulation of the flow structure by progressive bedforms in the Kinoshita meandering channel, Earth Surf. Process. Landforms 38, 1612–1622. DOI: 10.1002/esp.3460.

Alexander, J., Bridge, J. S., Cheel, R. J., Leclair, S. F. 2001. Bedforms and associated sedimentary structures formed under supercritical water flows over aggrading sand beds, Sedimentology, 48(1) : 133-152. DOI:10.1046/j.1365-3091.2001.00357.x.

Bromley, J. C. 2007. The morphodynamics of sediment movement through a reservoir during dam removal, PhD thesis, University of Nottingham, UK.

Cartigny, M. J. B., Ventra, D., Postma G., van Den Berg, J. H. 2014. Morphodynamics and sedimentary structures of bedforms under supercritical-flow conditions: New insights from flume experiments, Sedimentology, 61(3) : 712-748. DOI:10.1111/sed.12076.

Curran, J. C. 2007. Step–pool formation models and associated step spacing, Earth Surface Processes and Landforms, 32 : 1611–1627. DOI:10.1002/esp.1589.

Dore, A., Bonneton, P., Marieu, V., Garlan, T. 2016. Numerical modelling of subaqueous sand dune morphodynamics, Journal of Geophysical Research: Earth Surface, DOI: 10.1002/2015JF003689.

Engelund, F., Hansen, E. 1967. A monograph on sediment transport in alluvial streams, Teknisk Forlag, Copenhagen, Denmark.

Fischer-Antze, T., Olsen, N. R. B., Gutknecht, D. 2008. Three-dimensional CFD modeling of morphological bed changes in the Danube River, Water Resources Research, 44(9) : W09422. DOI: 10.1029/2007WR006402.

Gilbert, G. K., 1914. The transportation of debris by running water. Geological Survey Water-Supply Paper, no. 86. U.S. Government Printing Office.

Giri, S., Shimizu, Y. 2006. Numerical computation of sand dune migration with free surface flow, Water Resources Research, 42(10) : W10422. DOI:10.1029/2005WR004588.

Haun, S., Olsen, N. R. B. 2012. Three-dimensional numerical modelling of reservoir flushing in a prototype scale, International Journal of River Basin Management, 10(4) : 341-349. DOI:10.1080/15715124.2012.736388.

Haun, S., Kjærås, H., Løvfall, S., Olsen, N. R. B. 2013. Three-dimensional measurements and numerical modelling of suspended sediments in a hydropower reservoir, Journal of Hydrology, 479(4) : 180-188. DOI:10.1016/j.jhydrol.2012.11.060.

Karim, F. 1999. Bed-form geometry in sand-bed flows, J. of Hydraulic Eng., 127(12) : 1253-1263. DOI:10.1061/(ASCE)0733-9429(1999)125:12(1253).

Kennedy, J. F. 1963. The mechanics of dunes and antidunes in erodible-bed channels, J. of Fluid Mech., 16 (4) : 521–544.

Kennedy, J. F. 1960. Stationary waves and antidunes in alluvial channels, PhD Thesis, California Institute of Technology, USA.

Launder, B. E., Spalding, D. B. 1974. The numerical computation of turbulent flows, Comput. Meths. Appl. Mech. Eng., 3 (2) : 269-289. DOI:10.1016/0045-7825(74)90029-2.

Lopes, A.M.G., Oliveira, L. A., Ferreira, A. D., Pinto, J. D. 2013. Numerical simulation of sand dune erosion, Env. Fluid Mech., 13 (2) : 145-168. DOI: 10.1007/s10652-012-9263-2.

Mewis, P. 2016. Formation of river dunes by measurement, stability analysis and simulation with Bmor3D, International Symposium on River Sedimentation, Stuttgart, Germany.

Nabi, M., De Vriend, H. J., Mosselman, E., Sloff, C. J., Shimizu, Y. 2013. Detailed simulation of morphodynamics: 3. Ripples and dunes, Water Resources Research, 49(9) : 5930-5943. DOI:10.1002/wrcr.20457.

Naqshband, S., van Duin, O., Ribberink, J., Hulscher, S., Modeling river dune development and dune transition to upper stage plane bed. Earth Surf. Process. Landforms 41, 323–335. DOI: 10.1002/esp.3789.

Núñez-González, F., Martín-Vide, J. P. 2010. Downstream-migrating antidunes in sand, gravel and sand-gravel mixtures, RiverFlow 2010, Braunschweig, Germany.

Núñez-González, F., Martín-Vide, J. P. 2011. Analysis of antidune migration direction, J. of Geophysical Res. – Earth Surface, 116, F02004. DOI:10.1029/2010JF001761.

Núñez-González, F. 2012. Bed load transport of sand-gravel mixtures with antidunes – flume experiments, PhD thesis, Technical University of Catalunya, Barcelona, Spain.

Olsen, N. R. B., Kjellesvig, H. M. 1999. Three-dimensional numerical modelling of bed changes in a sand trap, J. of Hydraulic Res., 37 (2) : 189-198.

Olsen, N. R. B. 2003. 3D CFD Modeling of a Self-Forming Meandering Channel, J. of Hydraulic Eng., 5 : 366-372. DOI:10.1061/(ASCE)0733-9429(2003)129:5(366).

Olsen, N. R. B. 2013a. Numerical modelling of sediment transport in hydropower reservoirs. Final report from NFR project 191035, Department of Hydraulic and Environmental Engineering, NTNU (In Norwegian).

Olsen, N. R. B. 2013b. Numerical Algorithms for Predicting Sediment Slides in Water Reservoirs, Electronic Journal of Geotechnical Engineering, 18 (Y) : 2013.496.

Olsen, N. R. B. 2015. Four free surface algorithms for the 3D Navier-Stokes equations, J. of Hydroinformatics, 17(6) : 845-856. DOI:10.2166/hydro.2015.012.

Olsen, N. R. B. 2016. Numerical modelling of antidune formation and propagation, International Symposium on River Sedimentation, Stuttgart, Germany.

Patankar, S. 1980. Numerical Heat Transfer and Fluid Flow, T. Francis & Taylor publishers.

Recking, A., Bacchi, V., Naaim, M., Frey, P. 2009. Antidunes on steep slopes, Journal of Geophysical Research: Earth Surface, 114 (4) : F04025. DOI:10.1029/2008JF001216.

van Rijn L. C. 1982. Equivalent roughness of alluvial bed, Journal of Hydraulic Engineering, 108(10) : 1215-1218.

Ruether, N., Olsen, N. R. B. 2007. Modelling free-forming meander evolution in a laboratory channel using three-dimensional computational fluid dynamics, Geomorphology, 89 : 308-319. DOI:10.1016/j.geomorph.2006.12.009.

Ruether, N., Olsen, N. R. B., Eilertsen, R. 2008. 3D modeling of flow and sediment transport over natural dunes, RiverFlow 2008, International Conference on Fluvial Hydraulics, Cesme, Izmir, Turkey, 2 : 1479-1485.

Schlichting, H. 1979. Boundary layer theory, McGraw-Hill Book Company, New York.

Stoesser, T., von Terzi, D., Rodi, W., Olsen, N. R. B. 2006. RANS simulations and LES over dunes at low relative submergence ratios, 7th Int. Conf. on Hydroscience and Engineering, Philadelphia, USA.

Tjerry, S., Fredsøe, J. 2005. Calculation of dune morphology, Journal of Geophysical Research: Earth Surface, 110(4) : F04013. DOI: 10.1029/2004JF000171.

Walker, I. J., Shugar, D. H. 2013. Secondary flow deflection in the lee of transverse dunes with implications for dune morphodynamics and migration. Earth Surf. Process. Landforms 38, 1642–1654. DOI: 10.1002/esp.3398.

Warmink, J. J., Dohmen-Janssen, M. C., Lansink, J., Naqshband, S., van Duin, O. J. M., Paarlberg, A. J., Termes, P., Hulscher, S. J. M. H. 2014. Understanding river dune splitting trough flume experiments and analysis of a dune evolution model. Earth Surf. Process. Landforms 39, 1208–1220. DOI: 10.1002/esp.3529.

Wilson C. A. M. E., Stoesser, T., Olsen, N. R. B., Bates, P. D. 2003. Application and Validation of Numerical Codes in the Prediction of Compound Channel Flows, Proceedings of ICE, Water, Maritime and Energy, 153 : 117-128.

Yokokawa, M., Hasegawa, K., Kanbayashi, S., Endo, N. 2010. Formative conditions and sedimentary structures of sandy 3D antidunes: An application of the gravel step-

pool model to fine-grained sand in an experimental flume, Earth Surface Processes and Landforms, 35(14) : 1720-1729. DOI:10.1002/esp.2069.

Zinke, P., Olsen, N. R .B., Bogen, J. 2011. 3D numerical modeling of levee depositions in a Scandinavian freshwater delta, Geomorphology, 129 : 320-333. DOI:10.1016/j.geomorph.2011.02.027.

Zijlema, V. 1996, On the construction of a third-order accrurate monotone convection scheme with application to turbulent flows in general domains, International Journal for Numerical Metods in Fluids, 22, 619-641

Case	Water depth	Flume length	Velocity	Froude number	Flume slope	Sediment diameter
5-1	10.5 cm	12 m	0.79 m/s	0.77	0.56 %	0.549 mm

Table 1. Key data from the flume study (Kennedy, 1960).

Vertical cells	Antidune length	Antidune height	Water depth	Anitidune celerity
38	0.37 m	2.1 cm	9.6 cm	7.3 mm/s
50	0.35 m	3.0 cm	10.8 cm	4.8 mm/s
Laboratory	0.38 m	2.7 cm *	10.5 cm	5 mm/s
Deviation	3-8 %	11-25 %	3-9 %	4-37 %

Table 2. Key results for the two grids and the laboratory experiments.

* The antidune height for case 5-1 was not measured in the laboratory. A value computed by the formula of Karim (1999) was used instead.

Figure 1. Partially breaking antidunes at the Bodendorf reservoir in Austria, during reservoir flushing (Olsen, 2013b).

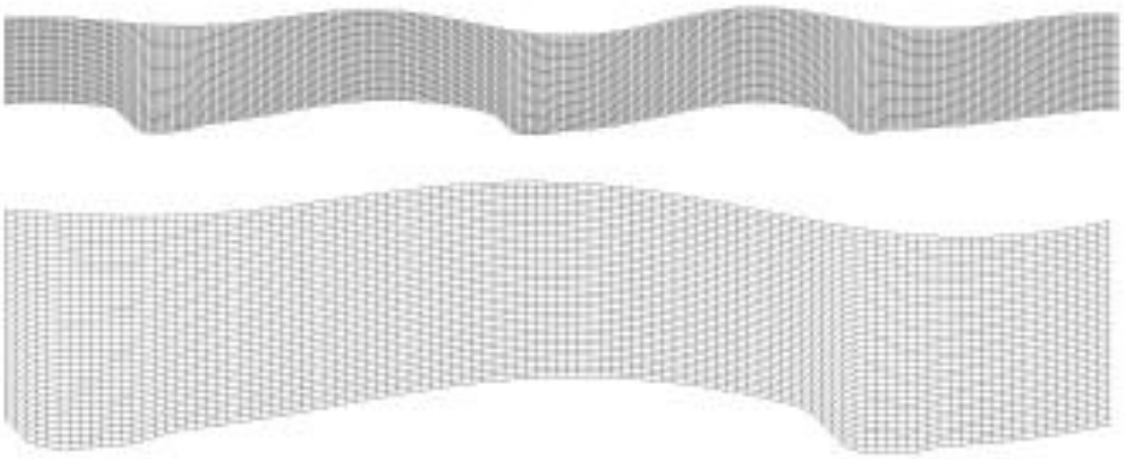

Figure 2. Longitudinal profiles of sections of the grid. The flow direction is from left to right.

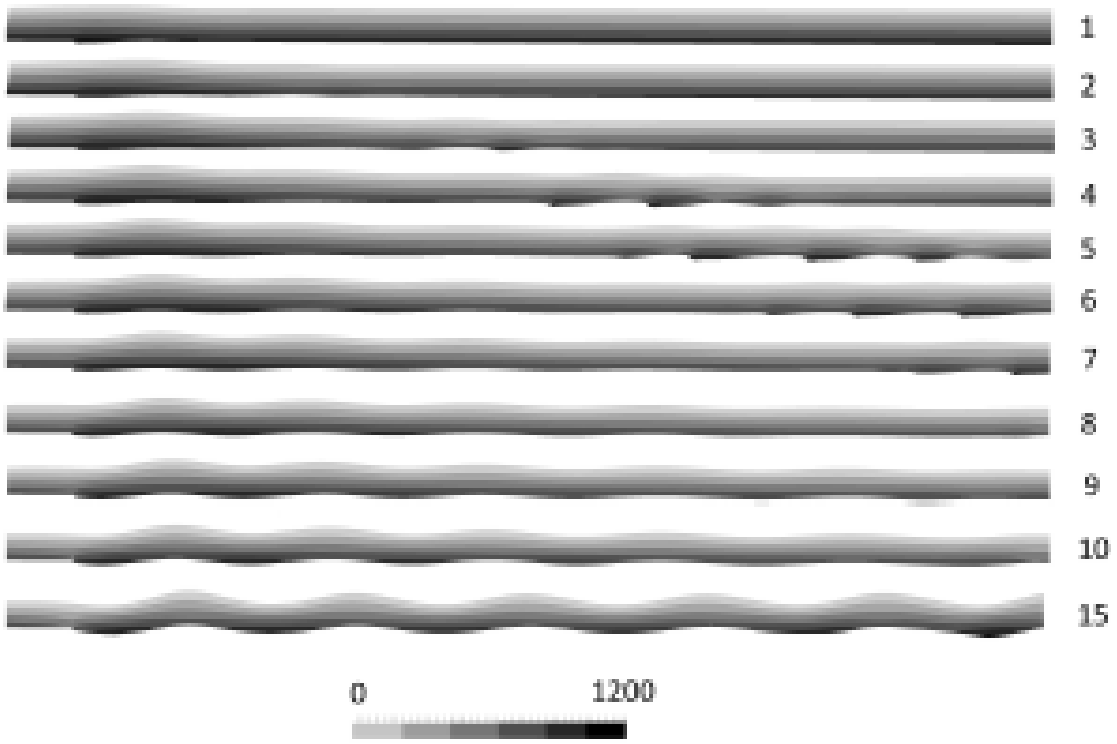

Figure 3. Development of the antidune formation. The greyshading scale shows the pressure in Pascal. The number at each figure is the time in seconds. The flow direction is from left to right.

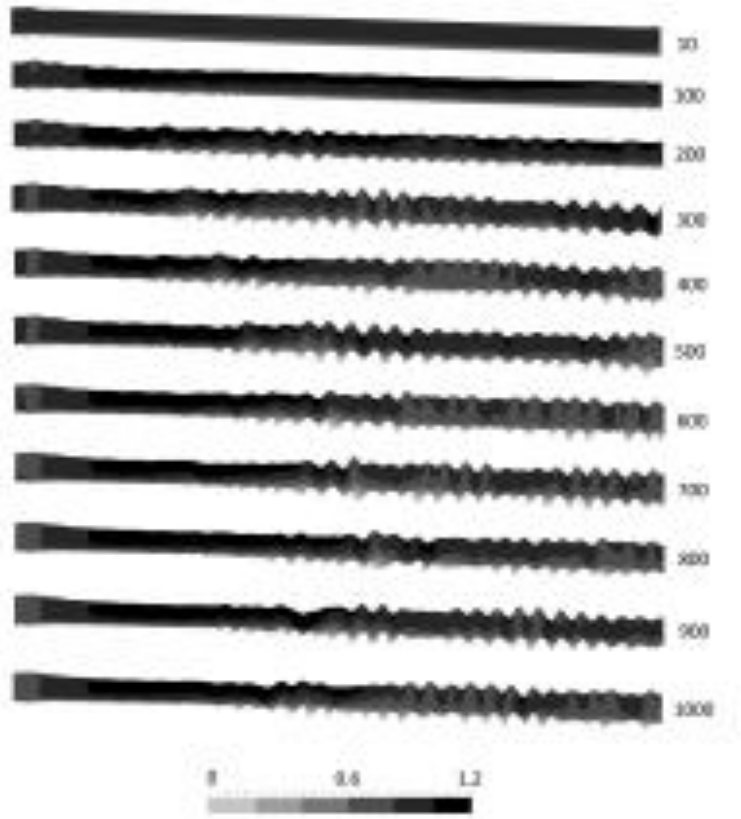

Figure 4. Longitudinal profiles at different times. The numbers indicate the time after the start of the run. The greyscale shows the computed velocities in m/s. The figures are distorted and 5x enlarged in the vertical direction.

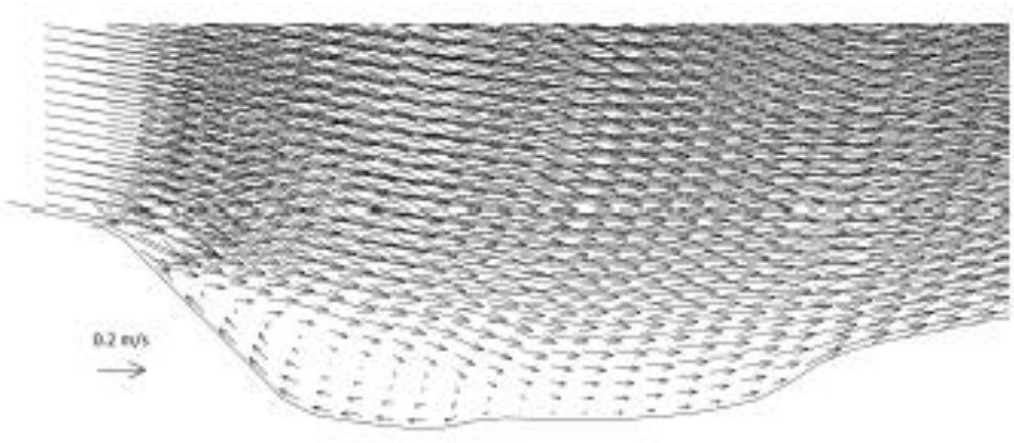

Figure 5. Velocity vectors showing a recirculation zone downstream of an antidune crest.

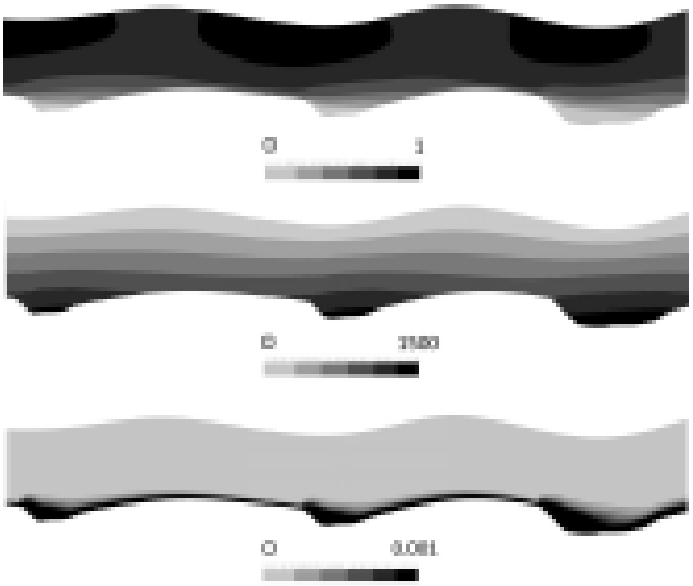

Figure 6. Longitudinal profiles of dunes, showing velocities (m/s, top), pressure (Pa, middle) and sediment concentrations (bottom).

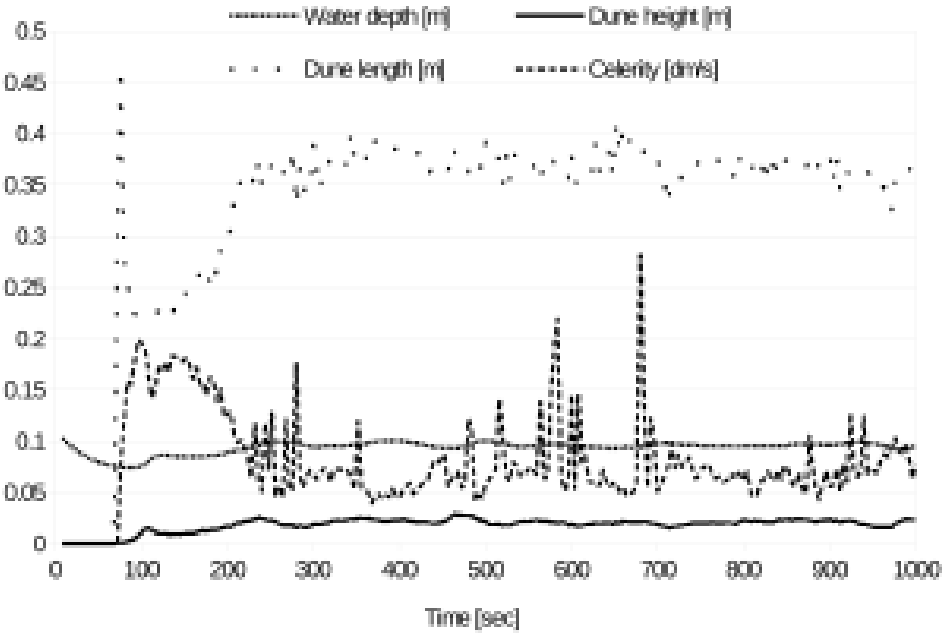

Figure 7. Time series of computed dune parameters for the grid with 38 cells in the vertical direction. The units on the vertical scale are given in the figure legends.

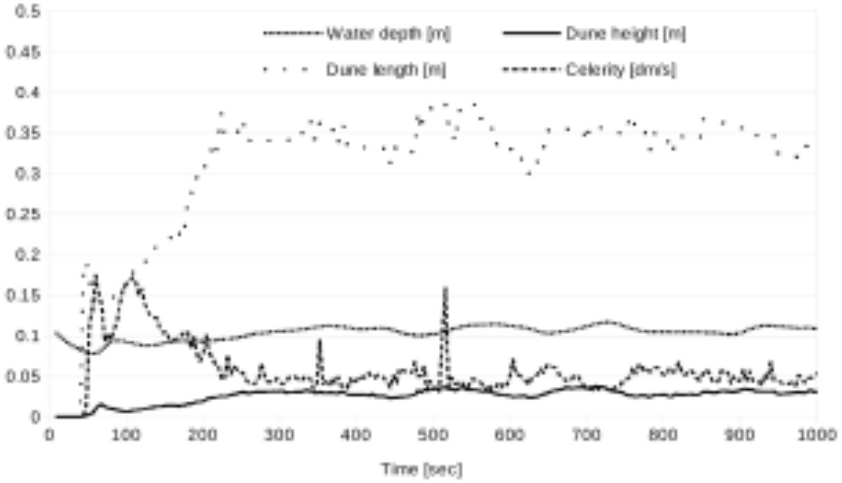

Figure 8. Time series of computed dune parameters for the grid with 50 cells in the vertical direction. The units on the vertical scale are given in the figure legends.

Figure 9. Longitudinal profile of a section of the grid computed with a time step of 0.0004 seconds instead of 0.0002 seconds.

Numerical modelling of downstream migrating antidunes

Nils Reidar B. Olsen

A 2D numerical model computing sediment transport together with solving the Navier-Stokes equations has been used to predict the formation and geometry of antidunes. The results correspond reasonably well with measurements from the laboratory for the parameters: dune height, dune length, water depth and dune celerity. The figure below shows velocity (m/s, upper figure), pressure (Pa, middle figure) and sediment concentration (fraction, lower figure).